PHYSICAL REVIEW C **95**, 061602(R) (2017)

Comprehensive ^{242m}Am neutron-induced reaction cross sections and resonance parameters

M. Q. Buckner,[1,*] C. Y. Wu,[1] R. A. Henderson,[1] B. Bucher,[1,2] N. Wimer,[1] A. Chyzh,[3] T. A. Bredeweg,[4] B. Baramsai,[4] A. Couture,[4] M. Jandel,[4] S. Mosby,[4] and J. L. Ullmann[4]

[1]*Lawrence Livermore National Laboratory, Livermore, California 94550, USA*
[2]*Idaho National Laboratory, Idaho Falls, Idaho 83415, USA*
[3]*North Carolina State University, Raleigh, North Carolina 27695, USA*
[4]*Los Alamos National Laboratory, Los Alamos, New Mexico 87544, USA*

(Received 25 April 2017; published 30 June 2017)

The ^{242}Am metastable isomer's neutron-induced destruction mechanisms were studied at the Los Alamos Neutron Science Center using the Detector for Advanced Neutron-Capture Experiments array with a compact parallel-plate avalanche counter. New ^{242m}Am neutron-capture cross sections were determined from 100 meV to 10 keV, and the absolute scale was set with respect to a concurrent measurement of the well-known ^{242m}Am neutron-induced-fission cross section. The new fission cross section spans an energy range from 100 meV to 1 MeV and was normalized to the ENDF/B-VII.1 evaluated cross section to set the absolute scale. Our ^{242m}Am(n,f) cross section agrees well with the cross section of Browne *et al.* [Phys. Rev. C **29**, 2188 (1984)] over this large energy interval. The new neutron-capture cross section measurement complements and agrees well with our recent results reported below 1 eV in Buckner *et al.* [Phys. Rev. C **95**, 024610 (2017)]. This new work comprises the most comprehensive study of ^{242m}Am(n,γ) above thermal energy. Neutron-induced resonance energies and parameters were deduced with the SAMMY R-matrix code for incident neutron energies up to 45 eV, and the new average Γ_γ is 13% higher than the evaluated average γ width.

DOI: 10.1103/PhysRevC.95.061602

The metastable isomeric state of ^{242}Am is unique, with attributes that make it suitable for numerous energy-related applications. With a 141(2) year half-life, ^{242m}Am occupies the 5^- excited state, the 48.60(5) keV energy level, before decaying by isomeric transition to the 1^- ground state [1]. The isomer is an attractive nuclear fuel because it is relatively long-lived with a significantly longer half-life than the ^{242}Am ground state: 16.02(2) hours [1]. Another appealing quality is that ^{242m}Am has the highest measured thermal-fission cross section of any known nucleus [2,3]; it is nearly an order of magnitude higher than the ^{235}U and ^{239}Pu cross sections at thermal energy. A broad, low-lying neutron-induced resonance at $E_{n,\mathrm{R}} = 178$ meV [4] is likely responsible for this extraordinarily high thermal-fission cross section [5]. These properties, coupled with the fact that ^{242m}Am provides more prompt-fission neutrons than conventional fuels [6], increase its appeal. Exotic and exciting applications, including a space reactor [7–16], a nuclear engine [17], a small-core reactor [18,19], and a fission battery [6,20–25], have been proposed that exploit these attributes. Many of these applications require micrometer-thick deposits of ^{242m}Am that enable fission products to be directly converted to electricity [6,21,25]. An impediment to exploring this technology is the availability of ^{242m}Am, and the high thermal-fission cross section is an *Achilles' heel* that inhibits large-scale production via ^{241}Am neutron capture [26].

The ^{242m}Am neutron-capture cross section also makes producing large quantities of the isomer challenging, and this destruction mechanism competes with neutron-induced production methods [14]. The ^{242m}Am(n,γ) cross section also factors into calculations of heavy actinide concentrations in nuclear fuel [27], nuclear waste recycling, and isotope production [5,28,29]. Recently, the neutron-capture cross section was directly measured at the Los Alamos Neutron Science Center (LANSCE) with the Detector for Advanced Neutron-Capture Experiments (DANCE) by Buckner *et al.* [30] from thermal to 1 eV. The capture-to-fission ratio was found to be 26(4)% from thermal to 0.1 eV in this recent study [30]. The Buckner *et al.* [30] study comprises the first measurement of the ^{242m}Am neutron-capture cross section above thermal energy.

The ^{242m}Am neutron-induced fission channel, on the other hand, has been well studied by accelerator experiments [5,31–33] and detonations [34,35]. The data of Browne *et al.* [5] and Fursov *et al.* [33] dominate the evaluated neutron-induced-fission cross sections due to their high precisions [36,37].

The current work is an extension of the Buckner *et al.* [30] ^{242m}Am neutron-capture cross section measurement. New, concurrent measurements of the ^{242m}Am(n,f) and ^{242m}Am(n,γ) cross sections were made at LANSCE using the DANCE array [38] in combination with a parallel-plate avalanche counter (PPAC) [39] for fission fragment detection. In this new study, the neutron-induced-fission cross section was measured from an incident neutron energy (E_n) of 100 meV to 1 MeV, and the neutron-capture cross section was measured from $E_n = 100$ meV to 10 keV. As in the previous study, the ^{242m}Am(n,f) cross section was normalized to the ENDF/B-VII.1 [37] fission cross section, and the ^{242m}Am(n,γ) cross section is reported with respect to the measured fission cross section. Additionally, the ^{242m}Am neutron-induced resonance energies ($E_{n,\mathrm{R}}$), γ widths (Γ_γ), neutron widths (Γ_n), and fission widths (Γ_f) for 106 resonances with energies between 0.15 and 45 eV were extracted using the R-matrix code SAMMY [40]. Much of the experiment and analysis details

*Corresponding author: buckner4@llnl.gov

were covered in Buckner *et al.* [30]; however, new experimental efficiencies, neutron-capture resonance parameters, and neutron-capture cross section results are reported below.

The DANCE array, 160 equal-volume, equal-solid-angle BaF_2 crystals arranged in a 4π geometry located at the LANSCE Lujan Neutron Scattering Center [41], was used in this study to measure ^{242m}Am neutron-induced cross sections. Measurements were carried out over 15 days with an ^{242m}Am PPAC target installed within DANCE. A duplicate PPAC assembly, containing a blank target, was placed within DANCE to measure backgrounds induced by scattered neutrons. Background measurements were fielded over five days and later subtracted from data collected in the inclusive data acquisition mode (referred to as the *inclusive mode* in this paper). The americium target was fabricated at Lawrence Livermore National Laboratory (LLNL) with the electroplating cell described in Ref. [42]. The mass of the double-sided, electroplated ^{242m}Am target was measured to be $\approx$100 μg enriched to 99.1%. The target had an $\approx$7.6 mm diameter active area, $\approx$24% smaller than the target diameter in Ref. [30]. This reduction in the active area was intended to increase target material exposure and activation. The ^{241}Am contamination in the sample was determined by mass spectrometry to be less than 1%.

The PPAC was assembled according to the configuration outlined in Ref. [30], and operated under the same pressure and voltage conditions. However, one major change was that higher purity, 99.99%, isobutane was used. Also, in another departure from the operating conditions reported in Ref. [30], the pulse height digitizer threshold for fission events was lowered to 50 mV in this new study. The high-purity isobutane and the lower pulse-height threshold increased the efficiency of the PPAC and removed the time-dependent efficiency degradation observed during the Buckner *et al.* [30] measurement.

The PPAC efficiency is related to the PPAC-DANCE coincidence condition and is a key quantity required to determine the fission cross section. The neutron-capture cross section, on the other hand, depends upon the total γ-ray energy ($E_{\rm sum}$) spectrum and the cluster multiplicity ($M_{\rm cl}$) measured by the DANCE array in the inclusive mode. To optimize the true-to-background ratio and improve the precision of the measurement, appropriate gates were set on these quantities, and detector efficiencies related to these gates were required to determine the cross section. Efficiencies for both the PPAC ($\epsilon_{\rm PPAC}$) and DANCE ($\epsilon_{\rm DANCE}$) are summarized here, and the procedure for determining detector efficiencies is provided by Buckner *et al.* [30] in more detail.

An $\approx$1.7 ns timing resolution was observed in the PPAC-DANCE coincident timing spectrum, and a 6-ns coincidence gate was set around the timing peak. The weighted mean of PPAC efficiencies over several incident neutron energy bins was determined to be 52.8(7)%, and this value is a factor of $\approx$1.6 higher than the PPAC efficiency in Ref. [30]. Following the time-alignment and energy calibration procedure outlined in Buckner *et al.* [30], DANCE γ-ray energies were summed over a narrow, 6-ns coincident time window. As in Ref. [30], the $E_{\rm sum}$ efficiency is the ratio between the peak area (5.0–6.0 MeV in this case) and the total area of the characteristic neutron-capture $E_{\rm sum}$ spectrum. Figure 1 shows the neutron-capture $E_{\rm sum}$ in orange over the incident neutron energy bin $E_n = 0.1$ to 1 eV and cluster multiplicities $M_{\rm cl} = (4,5)$. In the figure, the blue spectrum represents the fission component (scaled by the PPAC efficiency), the green spectrum is the presampled background (see Refs. [30,43]), and the purple spectrum is the environmental background. These three spectra were subtracted from the inclusive $E_{\rm sum}$ (dashed red) to reveal the characteristic ^{242m}Am neutron-capture signature identified by its 6364.9 ± 1.4 keV neutron separation energy [44]. The weighted mean of $E_{\rm sum}$ efficiencies over several incident neutron energy bins was found to be 35(4)% for cluster multiplicities $M_{\rm cl} = (4,5)$. The multiplicity efficiency was then calculated for different incident neutron energy bins below 10 eV, and the weighted mean, 30.4(15)%, was adopted as the detector multiplicity efficiency for $M_{\rm cl} = (4,5)$. The DANCE array efficiency is the product of the $M_{\rm cl}$ and $E_{\rm sum}$ efficiencies, and for $M_{\rm cl} = (4,5)$, $\epsilon_{\rm DANCE} = 10.7(14)\%$ in this study and is consistent with the efficiency derived in Ref. [30]. The observation made in Ref. [30], that values determined with respect to $M_{\rm cl} = (4,5)$ were more reliable, was confirmed in this new study, and as a result, the $M_{\rm cl} = (4,5)$ DANCE efficiency was used to evaluate the ^{242m}Am(n,γ) cross section.

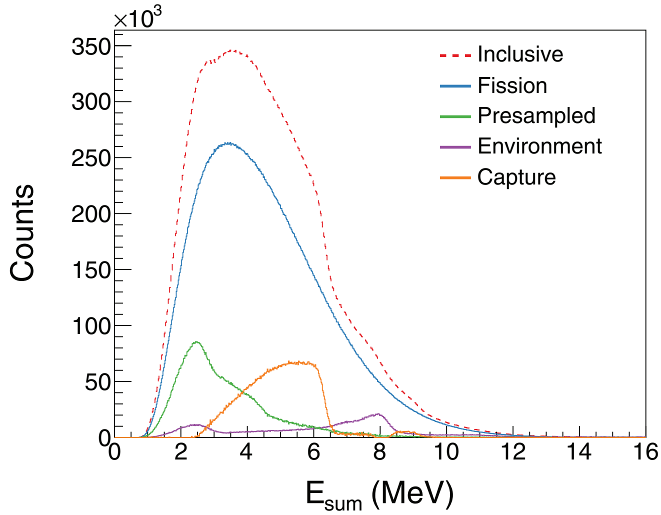

FIG. 1. The characteristic neutron-capture reaction channel $E_{\rm sum}$, shown in orange, after the subtraction of the fission (blue), presampled (green), and environmental (purple) spectra from the inclusive (dashed red) $E_{\rm sum}$. The spectra for the incident neutron energy bin 0.1–1 eV, with cluster multiplicities 4 and 5, are shown. Negative values and $E_{\rm sum}$ uncertainties are not shown in this figure to make it easier to distinguish between subtraction components.

Figure 2 shows the data quality for different incident neutron energy bins spanning $E_n = 1$ eV to 1 keV with cluster multiplicities $M_{\rm cl} = (4,5)$. The data quality deteriorated for the ^{242m}Am(n,γ) reaction as incident neutron energies exceeded 100 eV, and it is clear from Fig. 2(c) that it becomes challenging to isolate the (n,γ) signal after excluding the background contributions. In the figure, the inclusive $E_{\rm sum}$ (red) and the scaled fission (blue), presampled (green), and environmental (purple) background spectra are shown.

Corrections, with respect to the detector efficiencies, to the capture and fission data are necessary before cross sections

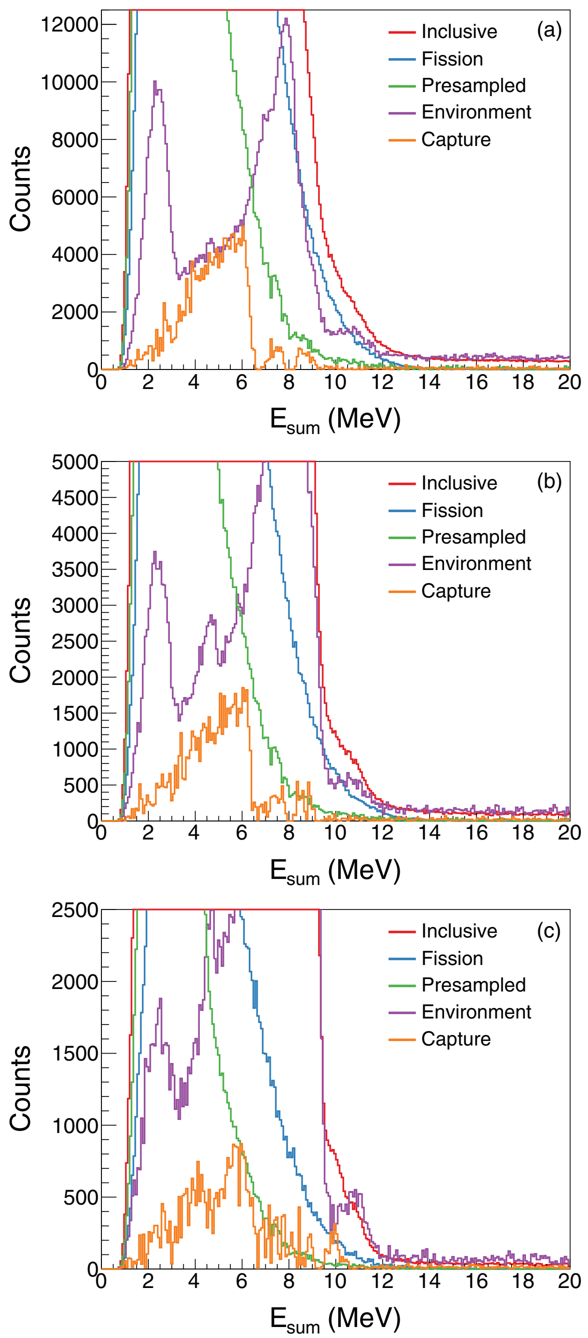

FIG. 2. The data quality for the ^{242m}Am(n,γ) reaction channel (orange) after fission (blue), presampled (green), and environmental (purple) background subtraction from the inclusive (red) spectrum. Incident neutron energy bins (a) 1–10 eV, (b) 10–100 eV, and (c) E_n = 100–1000 eV with cluster multiplicities 4 and 5 are shown. Negative values and E_{sum} uncertainties are not shown here to allow the subtraction components to be easily distinguished, but are included in the final analysis.

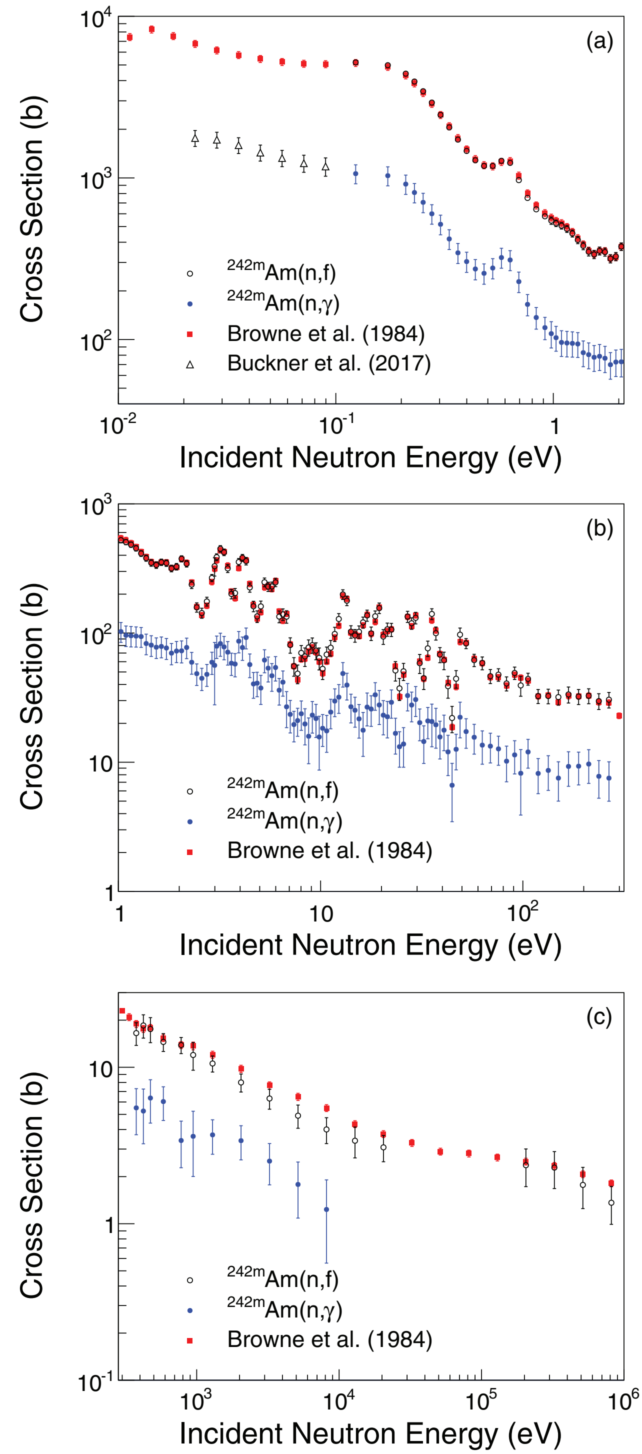

FIG. 3. The current ^{242m}Am(n,γ) cross section (filled blue circles) and the ^{242m}Am(n,f) cross section (open black circles) are plotted alongside the Browne *et al.* [5] (red squares) data for incident neutron energy ranges of (a) 10 meV to 2 eV, (b) 1 eV to 300 eV, and (c) 300 eV to 1 MeV. The neutron-capture cross sections <100 meV from Buckner *et al.* [30] (open black triangles), are included in (a). The fission cross section between 1 and 20 keV trends lower than that of Browne *et al.* [5] by ≈20%, but all reported values are within 1.5 standard deviations of the previous measurement. Excluded cross sections at ≈300 eV and ≈25 keV coincide with aluminum resonances.

can be determined. The absolute scale of the ^{242m}Am(n,f) cross section was set by normalizing the relative cross section to the evaluated cross section [37] over E_n = 100 meV to 50 eV. The new absolute fission cross section (open black circles) is shown in Fig. 3 alongside the Browne *et al.* [5]

TABLE I. Comparison between the current ^{242m}Am(n,γ) and ^{242m}Am(n,f) resonance parameters determined from the measured cross sections and the R-matrix code SAMMY [40] alongside the resonance energies and widths reported in ENDF/B-VII.1 [37]. Statistical uncertainties are quoted in the table. Note, in ENDF/B-VII.1 [37], the γ width for each resonance is 50 meV.

$E_{n,\mathrm{R}}$ (eV)		Γ_γ (meV)	Γ_n (meV)		Γ_f (meV)	
Present	[37]	Present	Present	[37]	Present	[37]
0.1778(2)	0.178	51.2(4)	0.2067(9)	0.1944	250.7(11)	244.5
0.6153(12)	0.615	56.0(12)	0.123(3)	0.111	196(4)	184
1.117(7)	1.10	132(5)	0.375(11)	0.424	770(20)	999
1.687(6)	1.71	66(4)	0.061(4)	0.050	233(13)	221
2.109(4)	2.11	81(3)	0.216(6)	0.181	345(10)	326
2.902(11)	2.95	66(5)	0.082(7)	0.082	220(16)	237
3.164(8)	3.18	56(3)	0.290(16)	0.273	299(14)	310
3.402(8)	3.39	59(4)	0.249(17)	0.242	262(14)	267
3.999(6)	4.013	57(3)	0.290(14)	0.266	232(11)	220
4.275(7)	4.27	60(4)	0.266(16)	0.234	213(12)	215
4.61(3)	4.55	67(5)	0.212(16)	0.231	490(40)	600
5.340(9)	5.37	82(4)	0.53(2)	0.53	361(18)	442
5.64(4)	5.7	50(5)	0.0478(5)	0.0468	186(17)	184
5.922(10)	5.95	63(4)	0.393(19)	0.356	302(17)	307
6.15(3)	6.15	55(5)	0.087(8)	0.081	210(20)	246
6.628(8)	6.65	56(4)	0.244(11)	0.214	220(14)	202
6.919(16)	6.84	45(5)	0.039(4)	0.038	78(7)	70
7.09(3)	7	51(5)	0.038(4)	0.036	111(11)	111
7.32(3)	7.21	62(5)	0.105(8)	0.104	320(30)	354
8.03(2)	8.07	74(6)	0.149(11)	0.131	310(30)	471
8.50(7)	8.6	57(5)	0.081(7)	0.073	400(40)	500
9.02(3)	9.03	72(6)	0.42(2)	0.41	640(50)	850
9.38(4)	9.43	58(5)	0.067(6)	0.057	125(13)	147
9.87(5)	9.88	60(5)	0.181(14)	0.159	460(40)	575
10.30(9)	10.3	52(5)	0.0146(14)	0.0138	84(9)	89
10.52(6)	10.62	56(5)	0.138(12)	0.124	340(30)	400
10.82(6)	10.87	54(5)	0.079(7)	0.073	166(15)	172
11.14(7)	11.25	54(5)	0.101(9)	0.095	360(40)	400
11.33(6)	11.43	57(5)	0.157(14)	0.137	230(20)	274
11.64(6)	11.79	53(5)	0.040(4)	0.038	96(10)	102
11.87(3)	11.92	63(5)	0.42(3)	0.36	320(30)	397
12.571(14)	12.62	66(5)	0.92(6)	0.81	290(20)	343
12.98(5)	13.04	58(5)	0.47(4)	0.43	250(20)	300
13.416(16)	13.41	64(5)	0.91(5)	0.86	320(30)	400
13.89(6)	13.9	55(5)	0.21(2)	0.21	260(30)	280
14.37(5)	14.42	60(5)	0.43(3)	0.40	390(40)	517
14.72(3)	14.68	60(5)	0.37(3)	0.33	360(40)	447
15.22(5)	15.15	52(5)	0.047(4)	0.045	68(7)	70
15.64(5)	15.67	60(5)	0.80(6)	0.79	520(40)	596
16.17(9)	16.06	50(5)	0.073(7)	0.072	160(16)	159
16.34(8)	16.48	55(5)	0.62(5)	0.61	550(50)	601
16.90(3)	16.92	64(5)	1.07(7)	0.99	490(50)	649
17.56(13)	17.5	56(5)	0.34(3)	0.31	340(40)	417
17.89(6)	17.82	55(5)	0.189(18)	0.176	200(20)	222
18.48(6)	18.47	63(5)	0.99(9)	0.96	490(50)	649
18.99(5)	19.07	59(5)	0.77(7)	0.72	400(40)	473
19.32(12)	19.31	54(5)	0.62(6)	0.58	360(40)	391
19.7(2)	19.7	54(5)	0.64(6)	0.59	390(40)	441
20.05(7)	20	54(5)	0.47(4)	0.44	250(30)	272
20.42(7)	20.3	55(5)	0.35(3)	0.34	300(30)	323
20.91(15)	20.9	52(5)	0.23(3)	0.23	470(50)	492
21.1(2)	21.15	52(5)	0.148(15)	0.147	260(30)	267
21.41(5)	21.46	57(5)	0.88(7)	0.89	500(50)	557
21.70(7)	21.8	52(5)	0.121(12)	0.116	68(7)	70
22.1(2)	22.15	56(5)	0.46(4)	0.42	310(30)	361
22.44(8)	22.5	63(5)	1.00(8)	0.94	500(50)	666
23.12(12)	23	56(5)	0.31(3)	0.30	450(50)	508
23.3(4)	23.3	51(5)	0.132(13)	0.133	890(90)	905
23.82(12)	23.65	53(5)	0.36(3)	0.36	800(80)	844
24.71(8)	24.65	51(5)	0.057(5)	0.054	69(7)	70
24.75(15)	24.92	51(5)	0.114(11)	0.109	210(20)	218
25.12(8)	25.1	51(5)	0.22(2)	0.21	210(20)	207
25.34(17)	25.38	51(5)	0.198(18)	0.187	176(17)	183
25.75(5)	25.68	53(5)	0.26(2)	0.25	280(30)	294
26.84(2)	26.99	68(5)	2.6(2)	2.3	330(30)	475
27.2(2)	27.15	51(5)	0.081(8)	0.081	260(30)	268
27.40(7)	27.4	57(5)	1.16(11)	1.10	380(40)	434
28.28(9)	28.45	56(5)	1.62(14)	1.63	660(70)	740
28.48(9)	28.75	52(5)	0.141(14)	0.135	67(7)	70
28.86(6)	29	56(5)	1.71(15)	1.70	560(60)	635
29.14(11)	29.4	53(5)	0.56(5)	0.53	166(16)	178
29.78(12)	29.75	55(5)	0.57(5)	0.53	201(19)	225
30.12(8)	30.08	56(5)	1.06(10)	1.03	440(50)	488
30.60(19)	30.55	54(5)	0.39(4)	0.38	360(40)	392
31.16(18)	30.98	53(5)	0.184(18)	0.175	250(30)	266
31.52(8)	31.55	54(5)	0.68(6)	0.65	460(50)	502
31.9(3)	32	53(5)	0.23(2)	0.22	360(40)	389
32.31(15)	32.35	52(5)	0.28(3)	0.27	310(30)	320
32.67(17)	32.85	52(5)	0.162(16)	0.157	230(20)	246
33.43(14)[a]	33.6	54(5)	0.32(3)	0.69	200(20)	815
33.66(19)[a]	33.85	53(5)	0.70(7)	0.30	770(80)	222
34.13(14)	34.08	50(5)	0.030(3)	0.029	83(8)	83
34.16(16)	34.2	53(5)	0.25(2)	0.23	130(13)	142
34.62(9)	34.7	52(5)	1.55(15)	1.49	740(70)	755
35.1(1)	35	49(5)	0.26(3)	0.26	90(9)	88
35.22(11)	35.33	50(5)	1.12(11)	1.09	340(30)	332
35.77(19)	35.88	53(5)	1.50(13)	1.45	440(40)	457
36.21(6)	36.35	53(5)	1.65(15)	1.62	580(60)	597
36.7(4)	36.65	51(5)	0.97(10)	0.96	850(80)	848
37.22(15)	37.1	51(5)	0.193(19)	0.190	115(12)	116
37.5(2)	37.52	54(5)	0.92(8)	0.88	290(30)	310
37.86(18)	37.85	53(5)	1.04(10)	1.02	530(50)	552
38.0(4)	38.3	51(5)	0.48(5)	0.48	810(80)	820
38.88(17)	38.9	52(5)	0.76(7)	0.76	660(70)	670
39.2(2)	39.25	52(5)	0.46(5)	0.46	280(30)	284
39.49(11)	39.6	51(5)	0.31(3)	0.30	93(9)	94
39.87(11)	39.95	53(5)	1.47(14)	1.44	520(50)	531
40.3(2)	40.4	52(5)	0.49(5)	0.48	270(30)	278
40.97(11)	40.8	50(5)	0.32(3)	0.31	220(20)	220
41.10(13)	41.18	50(5)	0.32(3)	0.32	94(9)	95
41.44(14)	41.45	50(5)	0.31(3)	0.31	70(7)	70
41.97(13)	41.68	51(5)	0.145(14)	0.141	99(10)	101
42.36(16)	41.9	52(5)	1.22(10)	1.12	920(80)	847
42.5(2)	42.62	51(5)	0.46(4)	0.45	350(40)	357
43.11(7)[a]	42.9	53(5)	0.27(3)	0.44	92(9)	823
44.95(16)[a]	43.3	51(5)	0.57(5)	0.26	850(80)	97

[a]Two pairs of adjacent resonances have swapped parameters, with respect to ENDF/B-VII.1 [37], due to the finite neutron energy resolution of the measurement.

neutron-induced-fission cross section (filled red squares). Note that the Browne *et al.* [5] data dominate the evaluated cross section [36,37]. Also, note that Fig. 3 includes the 5% systematic uncertainty on the data from Ref. [5]. The new measurement agrees well with the literature value up to $E_n \approx 1$ MeV. The neutron-induced reaction cross sections, including the fission channel, were excluded at 300 keV and above 25 keV due to the significant neutron flux loss from neutron-induced reactions on aluminum and manganese in the entrance window. The absolute neutron-capture cross section was extracted with respect to the new absolute fission cross section and is plotted alongside the fission cross sections in Fig. 3 from 100 meV to 10 keV (filled blue circles). The capture cross sections from thermal energy to 0.1 eV reported by Buckner *et al.* [30] (open black triangles) are included in Fig. 3(a).

In addition to the measured cross sections, the ^{242m}Am neutron-induced resonance energies as well as neutron, fission, and γ widths for 106 resonances with energies between 0.15 and 45 eV were determined with the R-matrix code SAMMY [40]. The initial conditions of the R-matrix calculation, including spins and parities, were set according to ENDF/B-VII.1 [37]. Using the new data, a sequence of R-matrix calculations was performed for the fission and capture cross sections, and this sequence was iterated to converge upon final widths based on the data. Resonance energies and widths based on both our new neutron-capture and neutron-induced-fission cross sections along with the parameters reported by ENDF/B-VII.1 [37] are tabulated in Table I. The average Γ_γ for resonance energies within the range 0.15–45 eV was found to be 56.5 meV, and this is ≈13% higher than the average estimated by ENDF/B-VII.1 [37]. Uncertainties quoted in Table I are statistical. Note that a few pairs of adjacent resonances in Table I have swapped parameters with respect to the evaluation [37] due to the finite neutron energy resolution of the measured cross sections.

Neutron-induced reactions on ^{242m}Am were studied with the DANCE array in conjunction with a compact PPAC for fission-fragment detection at the LANSCE Lujan Neutron Scattering Center. A new ^{242m}Am(n,f) cross section was derived for E_n from 100 meV to 1 MeV and agrees well with previous measurements. A new absolute ^{242m}Am(n,γ) cross section was obtained, for E_n from 100 meV to 10 keV, with respect to the new fission cross section. These results represent the most comprehensive direct measurement of the ^{242m}Am(n,γ) reaction above thermal energy and complement our previous results below 1 eV reported in Buckner *et al.* [30].

This new (n,γ) cross section will have important implications for simulations of ^{242m}Am-based propulsion and energy systems. Additionally, this extension of the Buckner *et al.* [30] measurement up to 10 keV, along with new Γ_γ, Γ_n, and Γ_f widths for 106 resonances with energies <45 eV, should impact and improve model calculations. These cross sections and widths should enable extrapolation of the neutron-capture cross section to higher incident neutron energies beyond the scope of this work.

This measurement was performed under the auspices of the U.S. Department of Energy by Lawrence Livermore National Security, LLC under Contract No. DE-AC52-07NA27344 and by Los Alamos National Security, LLC under Contract No. DE-AC52-06NA25396. Additional funding was provided by the U.S. DOE/NNSA Office of Defense Nuclear Nonproliferation Research and Development.

[1] Y. A. Akovali, Nucl. Data Sheets **96**, 177 (2002).
[2] E. K. Hulet, R. W. Hoff, H. R. Bowman, and M. C. Michel, Phys. Rev. **107**, 1294 (1957).
[3] K. Wolfsberg, G. P. Ford, and H. L. Smith, J. Nucl. Energy, Parts A/B **20**, 588 (1966).
[4] S. F. Mughabghab, *Atlas of Neutron Resonances: Resonance Parameters and Thermal Cross Sections. Z = 1–100* (Elsevier, New York, 2006).
[5] J. C. Browne, R. M. White, R. E. Howe, J. H. Landrum, R. J. Dougan, and R. J. Dupzyk, Phys. Rev. C **29**, 2188 (1984).
[6] Y. Ronen, M. Kurtzhand, L. Droizman, and E. Shwageraus, J. Propul. Power **23**, 874 (2007).
[7] Y. Ronen and M. J. Leibson, technical report, Technion, Israel Institute of Technology, Department of Nuclear Engineering, 1987 (unpublished), p. 42.
[8] Y. Ronen and M. J. Leibson, Nucl. Sci. Eng. **99**, 278 (1988).
[9] G. Chapline, Nucl. Instrum. Methods Phys. Res., Sect. A **271**, 207 (1988).
[10] H. Ludewig, O. Lazareth, S. Mughabghab, K. Perkins, and J. R. Powell, Small propulsion reactor design based on particle bed reactor concept, Technical Report, Brookhaven National Laboratory, 1989 (unpublished).
[11] T. Kammash, D. L. Galbraith, and T.-R. Jan, in *Proceedings of the 10th Symposium on Space Nuclear Power and Propulsion, Albuquerque, NM*, AIP Conf. Proc. No. 271 (AIP, New York, 1993).
[12] C. Rubbia, in *Proceedings of The Ninth International Conference on Emerging Nuclear Energy Systems, Keynote, Tel-Aviv, Israel* (International Atomic Energy Agency, Vienna, 1998), p. 4.
[13] Y. Ronen and E. Shwageraus, Nucl. Instrum. Methods Phys. Res., Sect. A **455**, 442 (2000).
[14] C. Rubbia, U.S. Patent No. 0,080,907 (28 March 2002).
[15] Y. Ronen and G. Raitses, Nucl. Instrum. Methods Phys. Res., Sect. A **522**, 558 (2004).
[16] M. Augelli, G. F. Bignami, and G. Genta, Acta Astronaut. **82**, 153 (2013).
[17] Y. Ronen, M. Aboudy, and D. Regev, Ann. Nucl. Energy **27**, 85 (2000).
[18] Y. Ronen, M. Aboudy, and D. Regev, Nucl. Technol. **129**, 407 (2000).
[19] Y. Ronen, M. Aboudy, and D. Regev, Nucl. Sci. Eng. **138**, 295 (2001).
[20] S. L. Soo, *Direct Energy Conversion* (Prentice-Hall, Engelwood Cliffs, NJ, 1968).
[21] G. H. Miley, Direct conversion of nuclear radiation energy, Technical Report, University of Illinois, Urbana-Champaign, 1970 (unpublished).

[22] G. Chapline and Y. Matsuda, Fusion Technol. **20**, 719 (1991).

[23] S. A. Slutz, D. B. Seidel, R. J. Lipinski, G. E. Rochau, and L. C. Brown, Phys. Plasmas **10**, 2983 (2003).

[24] P. V. Tsvetkov, R. R. Hart, and T. A. Parish, in *Proceedings of the 11th International Conference on Nuclear Engineering (ICONE 11)* (Japan Society of Mechanical Engineers, Tokyo, 2003), pp. 20–23.

[25] Y. Ronen, A. Hatav, and N. Hazenshprung, Nucl. Instrum. Methods Phys. Res., Sect. A **531**, 639 (2004).

[26] A. Cesana, S. T. Mongelli, M. Terrani, P. Benetti, E. Calligarich, R. Dolfini, and G. L. Raselli, Nucl. Technol. **148**, 97 (2004).

[27] J. L. Crandall, in *Proceedings of the International Conference on Constructive Uses of Atomic Energy, Washington, D.C.* (American Nuclear Society, La Grange Park, IL, 1968), p. 193.

[28] S. Raman, in IAEA advisory group meeting on transactinium isotope nuclear data, Karlsruhe, F.R. Germany, technical report,1975 (unpublished), p. 39.

[29] N. Shinohara, Y. Hatsukawa, K. Hata, and N. Kohno, J. Nucl. Sci. Technol. **34**, 613 (1997).

[30] M. Q. Buckner, C. Y. Wu, R. A. Henderson, B. Bucher, N. Wimer, A. Chyzh, T. A. Bredeweg, B. Baramsai, A. Couture, M. Jandel *et al.*, Phys. Rev. C **95**, 024610 (2017).

[31] C. D. Bowman, G. F. Auchampaugh, S. C. Fultz, and R. W. Hoff, Phys. Rev. **166**, 1219 (1968).

[32] J. W. T. Dabbs, C. E. Bemis Jr, S. Raman, R. J. Dougan, and R. W. Hoff, Nucl. Sci. Eng. **84**, 1 (1983).

[33] B. I. Fursov, B. F. Samylin, G. N. Smirenkin, and V. N. Polynov, in *Proceedings of the International Conference on Nuclear Data for Science and Technology, Gatlinburg, TN* (American Nuclear Society, La Grange Park, IL, 1994), Vol. 1, p. 269.

[34] P. A. Seeger, A. Hemmendinger, and B. C. Diven, Nucl. Phys. A **96**, 605 (1967).

[35] E. V. Fomushkin, G. F. Novoselov, Y. I. Vinogradov, V. V. Gavrilov, V. I. Inkov, B. K. Maslennikov, V. N. Polynov, V. M. Surin, and A. M. Shvetsov, Sov. J. Nucl. Phys. **33**, 620 (1981).

[36] P. Talou, T. Kawano, P. G. Young, M. B. Chadwick, and R. E. MacFarlane, Nucl. Sci. Eng. **155**, 84 (2007).

[37] M. B. Chadwick, M. Herman, P. Obložinský, M. E. Dunn, Y. Danon, A. C. Kahler, D. L. Smith, B. Pritychenko, G. Arbanas, R. Arcilla *et al.*, Nucl. Data Sheets **112**, 2887 (2011).

[38] M. Heil, R. Reifarth, M. M. Fowler, R. C. Haight, F. Käppeler, R. S. Rundberg, E. H. Seabury, J. L. Ullmann, J. B. Wilhelmy, and K. Wisshak, Nucl. Instrum. Methods Phys. Res. Sect. A **459**, 229 (2001).

[39] C. Y. Wu, A. Chyzh, E. Kwan, R. A. Henderson, J. M. Gostic, D. Carter, T. A. Bredeweg, A. Couture, M. Jandel, and J. L. Ullmann, Nucl. Instrum. Methods A **694**, 78 (2012).

[40] N. M. Larson, Oak Ridge National Laboratory Technical Report No. ORNL/TM-9179 **7**, 2006 (unpublished).

[41] P. W. Lisowski, C. D. Bowman, G. J. Russell, and S. A. Wender, Nucl. Sci. Eng. **106**, 208 (1990).

[42] R. A. Henderson, J. M. Gostic, J. T. Burke, S. E. Fisher, and C. Y. Wu, Nucl. Instrum. Methods Phys. Res., Sect. A **655**, 66 (2011).

[43] S. Mosby, T. A. Bredeweg, A. Chyzh, A. Couture, R. Henderson, M. Jandel, E. Kwan, J. M. O'Donnell, J. Ullmann, and C.-Y. Wu, Phys. Rev. C **89**, 034610 (2014).

[44] M. Wang, G. Audi, A. Wapstra, F. Kondev, M. MacCormick, X. Xu, and B. Pfeiffer, Chin. Phys. C **36**, 1603 (2012).